Journal of Mines, Metals and Fuels, *71(9): 1310-1328; 2023. DOI: 10.18311/jmmf/2023/35457*

Print ISSN : 0022-2755

Journal of Mines, Metals and Fuels

**Contents available at:** *www.informaticsjournals.com/index.php/jmmf*

# A Review on Thermal Modelling of Residual Stresses during Additive Manufacturing

**N. Chethan Kumar and Suyog Jhavar**

*School of Mechanical Engineering, VIT-AP University, Inavolu, Beside AP Secretariat, Amaravati – 522237, Andhra Pradesh, India; Suyog.jhavar@vitap.ac.in*

## Abstract

*Additive Manufacturing (AM) has received interest since it is simpler to manufacture complicated 3D component without the requirement for casting moulds than convective fabrication. AM has a lot of significance in fields like aerospace, medicine, and more to make parts of any kind of complex shape. Since the finished products are subjected to repeated cycles of heating and cooling, there will always be some residual stresses present in them. During layer-over-layer deposition, the large difference in temperature between the layers causes residual stresses, which hurt the performance of the products. As far as the author's knowledge, there is no thorough review of the thermal modelling of residual stress in AM. In this review paper, the goal is to first get a good understanding of how residual stresses are developed, and then to look at how different models measure them. So, residual stresses can be seen as a key factor in controlling costs, performance, and quality standards of the finished component. This paper does a thorough review of the field to give engineers and researchers up-to-date information and advice about residual stresses.*

**Keywords:** *Additive Manufacturing, Mechanical Modelling, Residual Stresses, Thermal Modelling*

## 1.0 Introduction

Additive Manufacturing (AM) is assuring approach of producing the final product by melting the input feeds that are in the form of metal wires or powder and accumulating it layer over layer pattern. AM technique is utilized to fabricate 3D complex profiles appropriate for certain vital applications but consistently accompanied by the generation of residual stresses[1]. The progressive effect of repeated heating and consecutive cooling process leads to large residual stresses in the component in addition leads the component to crack and delamination[2]. Residual stresses will endanger the productive life of the component affecting the whole structure to collapse. Numerous experimental techniques are applied to identify residual stress that is destructive and non-destructive in nature after the printing of the final component is done. Out of the many methods[2], XRD is a precise and commercially used non-destructive method in the market. In this method, residual stress measured in terms of strain in the crystalline lattice. In the Crack Compliance Technique (CCM)[3], the residual stresses are analysed by initiating an artificial crack in the component. In the concept of CCM, a straightforward correlation between residual stresses $\sigma_{rs}(x)$ and deformation strain concerning the factor of stress intensity is been obtained. The factor of stress intensity given in Equation (1) is influenced by residual stresses is given by $K_{sif}$[3].

$$K_{sif}(a) = \int_0^a h(x,a)\,\sigma_{rs}(x)dx \qquad (1)$$

Where $K_{sif}$ is the stress intensity factor, is the weight function and is the residual stresses through the cracking plane.

**Author for correspondence*

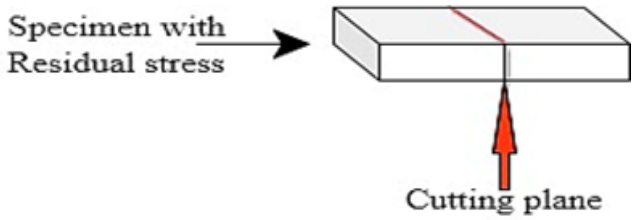



**Figure 1.** Contour technique specimen and cutting plane.

The contour method[4] is another technique to measure residual stress as shown in Figure 1. In the method, specimen-possessing residual is cut across in half by Electro-Discharge Machining (EDM). A 3D finite element analysis is executed in one of the cut specimens by applying boundary conditions and measuring normal stress components in order to calculate the specimen's residual stresses.

The sharp indentation method[5] is alternative non-destructive approach to determining residual stress. For this method to work, the basic premise is that residual tension is sensitive to even a little scrape, as shown in Figure 2. Three conditions are no residual stress projected area ($A_N$), tensile residual stress projected area ($A_T$) and compressive residual stress projected area ($A_C$).

The corresponding residual stress is classified by the indentation variable ($I^2$). Correspondingly if $I^2<1$ then the residual stresses are tensile in nature and if $I^2>1$ it's compressive residual stress.

Where $I^2 = \frac{A}{A_N}$ & A = Normal area of contact with no residual stress.

The sequential hole drilling approach[6] which is semi-destructive, involves drilling a hole through the material's structure in stages. This approach is particularly prone to errors in the experiments. Uncertain stress data can occur from any measurement, precondition formulation, or experimental equipment design problem. Finite element simulation is used to monitor relaxation deformations at the opening and calculate calibration coefficients, which are then used to measure the condition of residual stresses throughout the materials. The impact functional approach[7] for eccentric openings is the best approach for controlling irregularity. When eccentricity is low, the impact functions for the eccentric openings provide outcomes similar to those of a concentric hole. Investigations using customized rosettes with more than three different strain gauges to determine parameters that are either ambiguous or challenging to assess.

The residual stresses thru the specimen layer have been estimated using the layer removal approach[8] as well as the X-ray diffraction approach. The substance was cleaned by electro polishing thin layers. By removing the substance, a flat surface is produced. Specimen and solution (electrolyte) are components of the DC electrical system for this operation. The specimen was coated with Lacomit varnish to isolate the region that would be polished in touch with the electrolyte. Barker's reagent (5 ml of fluoroboric acids in 200 ml of $H_2O$ (water)) was used for the electro polishing, which was done at room temperature with 30V and 1A as the ideal voltage and current.

The film thickness that was eliminated during the electro polishing test in each increment in sequence to do

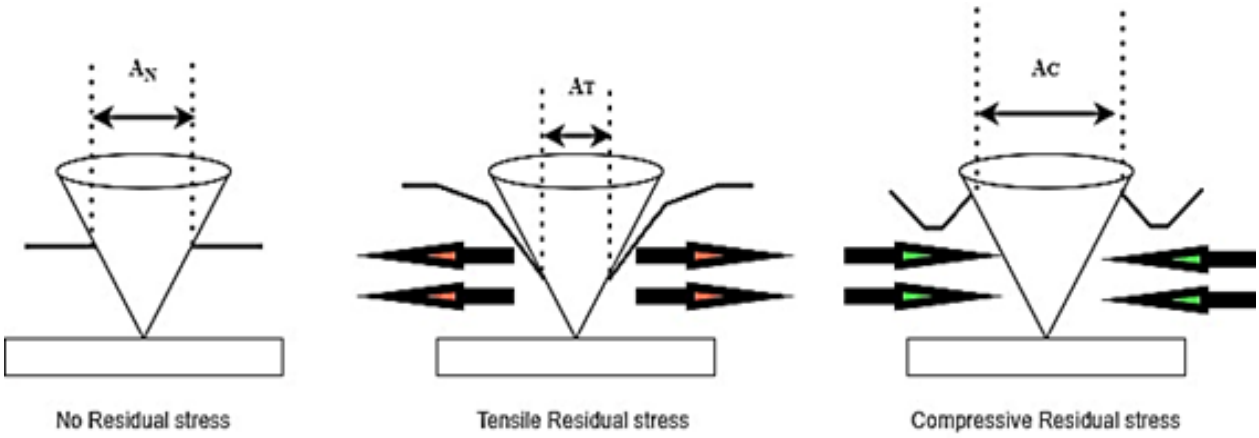



**Figure 2.** Sharp indentation technique specimen and projecting areas.

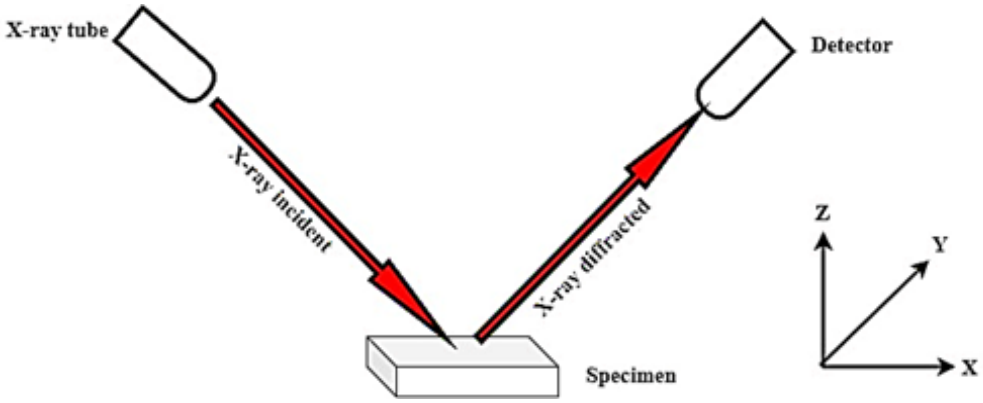



**Figure 3.** Schematic representation of X-Ray Diffraction.

the surface removal was 0.2 mm. A micrometre was been utilized to measure the thickness in every increment. Prior to performing the layer elimination technique, the surface residual stress absolute values were determined using the X-ray diffraction[9] method. In each increment, the stresses were measured in the longitudinally (x) and transversal (y) axes. The design for stress assessment using X-Ray Diffraction (XRD) is shown in Figure 3.

The layer removal approach is a low-cost and speedy way for testing the ferrite stress in cold-drawn pearlitic wires. This process allows for the stress evaluation to be finished with high accuracy in only a few minutes[10]. The stress patterns with in ferrite content in cold-drawn wires may be quantitatively quantified by using the layer removal strategy over the whole length of the wires, eliminating the requirement for more sophisticated diffraction mechanisms like X-Ray Diffraction. The steel cables have been under strain at the interface and compression inside the layer along a longitudinal axis, as seen by the XRD data, although the stress levels in the rods were minimal before cold drawing.

Among all these approaches, XRD is a trusted and widely used non-destructive method for estimating out residual stress. By detecting strain within the crystalline lattice, the XRD technique ambiguously estimates residual stress[11].

## 2.0 The Evolution and Transmission of Residual Stress

The wire input-form laser additive technology[12], which is unique for its exceptional flexibility and efficacy, is commonly used in large-scale structure. However, large-scale impacts and the resulting build-up of heat input lead to build severe stress and deformation inside such structures. In this research, we introduced a novel model for the stress development in thermal fluid mechanics in laser additive manufacturing. This paper describes an accurate numerical mapping method for connecting the CFD result to the FEM model. This model enables precise stress distribution measurement during the forming process as well as excellent cracking prediction. The new model merged the CFD model with the Finite element model. The CFD simulation accounted for wire melting, molten hot pool motion, and heat exchange. The Finite Element Model accounted for the influence of thermal stress on shape and temperature distribution.

We are able to investigate how the stress imposed on a system varies according to its morphology by making use of a newly developed thermal fluid mechanical model. The angle between both the vertical surface as well as the sidewall of such aggregation has a significant impact on the residual Mises stress, which is particularly sensitive to this angle. The simulation findings demonstrate that the surface formation quality has a significant impact on residual stress, particularly when acute flaws are present. A crack may occur if the tensile stress along the path of expansion is more than 800MPa. It is possible to achieve the outcome shown in the paper's example at a pressure of around 1100MPa/rad.

Curing residual stress[13] experimental measurement is frequently expensive and challenging. This study presents a multi-scale model as an option for those wishing to anticipate the distribution of residual stress in composites during the curing process. So to generate more accurate microscopic residual stresses, the research presented

here advises using a multi-scale technique to link the component and fiber-matrix levels.

In the beginning, a Three-Dimensional (3D) macroscopic scale model has been constructed in order to explain the component level temperatures, degrees of cures, macroscopic residual stresses, and strains. When it comes time to calculate the micro residual stresses, the information gleaned from the component level simulation is used as constraints in the Representational Volume Elements (RVE) model, which accounts for resin viscoelastic behaviour. The primary emphasis of this study is on the potential impact of boundary conditions that are relevant to real-world engineering challenges on the microscopic residual stresses for composite materials.

The macro viewpoint examines composites as though they were continuous media. The macro-scale model will be used to determine the temperature, cures degrees, macro-residual stresses, and strains. The authors study microscopic residual stresses in fibres, resin, and interphase while accounting for resin viscoelastic behaviour by include temperature, curing degree, and mechanical macroscopic residual strains predicted by the macro-scale model. To estimate the microscopic residual stresses in healing polymer-matrix composites, a multiscale model was developed. The micro residual stresses within the matrix and interphase will be exaggerated in simulations utilising mechanical symmetry boundary conditions.

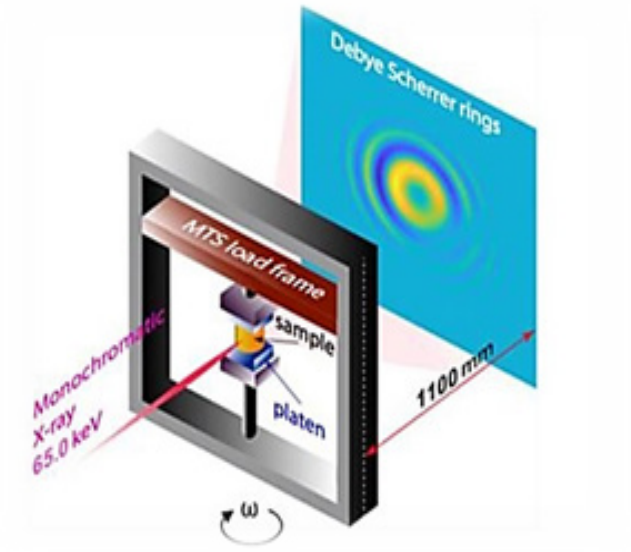



**Figure 4.** Experimental setup for collecting X-ray diffraction[14].

A sophisticated Elastic-Plastic Self-Consistent (EPSC)[14] crystalline plasticity model is used to provide predictions about the evolution of texturing, twinning, elastic lattice stresses, and flow stress as shown in Figure 4. Calibration is performed using a portion of the data set, and the model is started using the texturing and residual stress measured experimentally from a cooling simulation. The present work focuses on in-situ enhanced X-ray diffract and crystalline plasticity modeling of deformation parameters during loading and reloading of Be, a material that already has received substantially less attention than other HCP metals.

The discussed study refines the MS-EPSC idea for HCP metals by accounting for latent hardening[15], dislocation dissolution under strain-path modification, and slip system-level backstress. The development of elastic lattice stresses also corresponds favourably with information obtained from in-situ high- strength x-ray scattering measurements made during compressive unloading and loading. The second phenomenon, however, is crucial for forecasting re-yielding. Mechanical behaviour under loading and reloading was predicted and investigated, together with the basic contributions of backstress, reverse dislocation gliding, and residual stresses.

The model uses a unique collection of single-crystal hardening variables to reflect the material's complex strain-path-change and strain rate-sensitive deformations, including the evolution of the appearance, twinning, layer stresses, fluid stress, and inhomogeneous hardening. Predictions may be improved by include latent hardness, back stress at the level of the slide system, and residual stress.

Because of the complex heating process involved in Wire and Arc Additive Manufacturing (WAAM)[16], residual stress is extremely challenging. A three-dimensional thermal-mechanical model developed based on MSC is presented in this work. The Marc algorithm was developed to assess the thermal stress transformation and residual stress dispersion in a GMA-melted metal's circular inter-pass single-deposition. In order to ensure the model's correctness, complementary experiments are conducted.

The arc's residual stress distribution is also studied, paying special attention to its features near the arc's beginning and its centre. The finite element software MSC is used to create a transient three-dimensional model.

Marc will analyse the GMA-based AM round thin-walled component for thermal stress growth and residual stress parameters. During the verification trials, the stresses in the foundation and any subsequent layers are measured. When the distribution of residual stresses in single-pass multi-layer accumulation is simulated and compared to experimental results, it is clear that the proposed model provides good predictions.

The following inferences may be drawn from the simulation results: As the thickness of a layer grows, there are fewer stress cycles that are equivalent. Depending on where you seem, the product's residual stress characteristic will seem quite different. The front layer preheats the back, and the back layer then provides a boost of heat to the front. The load placed on the front layer is also relieved by the back layer. The residual stress along the length of a material is always in the large tensile state and is generally higher than the residual stress along the transverse axis and the axial axis.

The study examines the primary variables influencing the residual stress concentration of cohesive samples collected from around the globe. Although all samples were retrieved using the same convenient sampling and a Japanese standard sampling[17], the residual efficient stress that was determined at various sites and depths varied significantly. The article looked at the key variables affecting. The following are some of the study's intriguing results:

1) Sample placement (p): The largest p is found in the sample that is positioned one-third of the way from the edge. The value of p has been determined using both the sample and the procedure of extrusion first from the sampling tube.

2) The amount of time between sampling and p measuring in addition to immediate assessment on the site, the p-value was assessed up to two years following the sample. It is discovered that the duration's impact on the p value is minimal if the samples was precisely kept.

3) Sample transportation: After placing the sampling tubes, all samples were transferred while still within the tubes.

Determine how melting residual stresses will be distributed along the thickness of the layer at the weldment, independent of the weld parameters. In addition, this experiment investigated how welding RS affected the beginning of cracking and how fatigue life was calculated. A probabilistic evaluation was deemed necessary, hence one was performed[18]. Residual Stresses (RS) in welds regardless of weld parameters literature has been combed for information on the pattern of weld residual stresses, specifically how they are distributed in the thickness direction immediately at weldment for welded connections. Studies of residual stresses, RS information redistribution for longitudinal, transversal, butt joint, K joint, and cross-shaped joints were required so that the shape of the weld RS distribution could be predicted based on the surface RS.

Based on the Voronoi approach[19], a random simulation of polycrystalline structure of the matrix is constructed. Two opposing factors- laser power as well as laser scanning speed- have a significant impact on the average stress distribution in the grains. This granular heterogeneity is a direct product of the Nano indentation process. Each Voronoi cell has a probability of receiving one of the seven different grain characteristics generated by a python programme.

A laser surfaces hardening model was used to calculate the thermal stress distribution as well as the temperature profile under a variety of different procedures. This model takes grain inhomogeneity into consideration. The pace at which the laser is scanned has a greater impact on the stress distribution of the matrix than the intensity of the laser. The statistical analysis of a distribution characteristics of residual heat stress within the matrix was carried out in order to identify the effect strategy of processing parameters on the laser hardening process. This was done so that we could pin down which specific processing factors had the most impact on the lasers hardening procedure.

For the first time, dynamical numerical analysis[20] is employed to determine the residual stress distribution in a cold roll-formed beams with sigma sections. The findings reveal that when residual stress is present, the sigma beam's ultimate load-bearing capacity is slightly decreased due to the stress concentration in the region weakening the resistance of the inner webs. Results from X-ray diffraction measurements were utilised to validate these preliminary FEA findings.

The longitudinal stress remains in the elastic zone even while the transverse force causes elasto - plastic development throughout the bending process, proving that the roll sets are configured correctly. FE study of the sigma beams of varying cross-sections shows that the maximum durability is marginally decreased by

integrating residual stress, and that the model which approached residual stress may acquire a greater match against the experimental results.

The condition of metal components used in industrial goods is evaluated and controlled in large part by residual stress. One of the most efficient ways to assess residual stress without destroying is using X-ray studies. Thru the Debye ring deformation[21] in such observations, the impact of residual stress upon this crystalline structure may be seen. The outcomes of the original synchrotron investigation, including the reference specimen's residual stress distribution as determined by the initial prototype setup. Additionally, we contrast laboratory measurements with those obtained from the synchrotron. We use electropolishing to scratch the specimen's surface.

To investigate the dispersion and formation of RS during the hybrid lasered arc welding process of AH36 steel, a Thermal-Metallurgical-Mechanical (TMM) model was developed using SYSWELD[22]. To examine how various factors could affect the Weld RS, a number of simulations were run. Different cooling rates have an impact on how the residual stress develops mostly by altering the microstructure of the weld. The experimental data and the numerical findings agreed quite well. By taking into account the normal "wine glass" weld pattern and the diluted rate throughout simulation, the computational precision was increased. When the transition temperature is relatively low, the volume shift brought on by the phase transition has the greatest impact on the residual stress.

An examination of how various weld groove designs affect the distribution of stress concentration in multi-pass 40 mm in thickness HSLA metal butt-welds is the focus of this study. The effect of a uniform residual stress distribution throughout was studied, and its effects on both symmetrical and asymmetrical double-V grooves were analysed[23]. After a number of unidirectional weld passes, the weld zone's residual stress in the tensile direction is significantly increased. It's possible that the transverse residual stress might be reduced by combining the applied tensioning force with the lateral tensioning force.

An Optimised Segmented Heat Source (OSHS)[24] model is suggested to increase the effectiveness and accuracy of the simulation analysis for the Laser Fusion of Powder Beds (LPBF) process. To verify the computational stability of the OSHS, the optimal element seed density was determined using a mesh dependence test. Several different Heat Source (HS) modelling approaches were chosen to evaluate one another. The OSHS model is validated by comparing the predicted stress values to the experimental results obtained from the X-Ray Diffraction (XRD) analysis of the 316L specimens in their as-built state.

First in-situ distributed measurements of Material Extrusion (MEX) thermoplastic residual stresses. This unique measurement device comprises of an Optical Backscatter Reflectometry (OBR)[25] interrogation unit coupled to an integrated fibre optic strain sensor. We expose and confirm the residual strain distribution in 3D-printed parts. Main residual strain processes and in-situ OBR sensing concepts are discussed. Experiments showed a 4-mm minimum measurement range and 0.15 mm spatial resolution. A study showed that in-situ OBR may identify unseen production problems. First measurement of solidification-induced MEX strain. An OBR interrogation device is embedded into the measuring system's single-mode optical fibre. The dispersed strain sensing along the optical fibre axis is made possible by Rayleigh backscattering. The process of noninvasively embedding objects from micro to macro scales is shown. The method detects production defects. For Single-Mode Fibres (SMF) longer than 25 mm, OBR may measure residual stresses on the spot. When Polylactide (PLA) exits the nozzle, it rapidly heats up and then cools, as captured by the IR camera. The stress resulting from raising an object to a certain height follows a parabolic curve. The maximum residual strain is at a height of one-third from the heat bed. The method claims to assess the quality of 3D-printed items.

## 3.0 Approaches Concerning Theoretical Prediction of Residual Stresses

The double phase DP600 steel behaviour is explained by a thermo-mechanical plasticity simulation study, which includes a hardening as well as a temperature sensitivity term. Investigated are the residual stresses of the DP600 lap welding joint. When residual stress simulation findings are compared to experimental

neutron diffraction observations, excellent agreement is discovered. A more extended form of the Equation (2) is known as the Johnson-Cook temperature model[26] (k = n = 1) can be seen in the suggested model:

$$F(T) = (1 - k.T^{*m})^n \qquad (2)$$

In order to analyse the elasto-plastic behaviour and residual stress distributions of the double phase steel DP600 joints and to simulate lap laser welding, a sequential connected thermo-mechanical FE model was constructed. With this multi-material approach, pure alumina is employed on the outside, while alumina-zirconia is sandwiched in between pure alumina layers having high compressive residual stresses. demonstrate the ability of the multi-material, Lithography-based Ceramic Manufacturing (LCM)[27] technology to create alumina ceramics with unprecedentedly high strength. The characteristic strength of the alumina multi-material system is more than 1 GPa, which is much higher than that of monolithic alumina (usually measured at 650 MPa). It is shown that complex 3D-printed ceramic systems may be created by combining additive manufacturing developments with a multi-material ceramics approach. Because cracks may propagate rapidly and result in sudden collapse, they pose the greatest danger to the stability of these materials. Researchers are given a number of options for minimising the likelihood of cracks forming in AM components. This study[28] concentrates on AM cracking and prevention strategies. There has been research on the raw materials, processing, results, production capacity, computational modelling, and uses of AM using Ni-based super alloys. Neutron diffraction has been employed by many different labs. The procedure for calculating residual stress using neutron diffraction is shown in Figure 5.

A two-scale system for predicting turning-induced residual stress[29]. This cutting-edge computational method may foretell, within a matter of hours, a residual stress situation brought on by longitudinal rotation. The study enhances the measurement and allocation for thermo-mechanical loadings, and it is applied to a realistic machined surface. Simulate the residual stress fields resulting from longitudinal turning. Instead of removing material in three dimensions with a sophisticated chip design, this novel method replicates similar thermo-mechanical loadings on the surface. A semi-analytical thermo-mechanical model[30] with Goldak heat sources shown in Figure 6 is created for wire arc additive manufacturing. The suggested model's correctness is tested by comparing both mechanical and thermal predictions with experimental observations and simulated results from a nonlinear transient model. The suggested model accurately predicts temperatures history

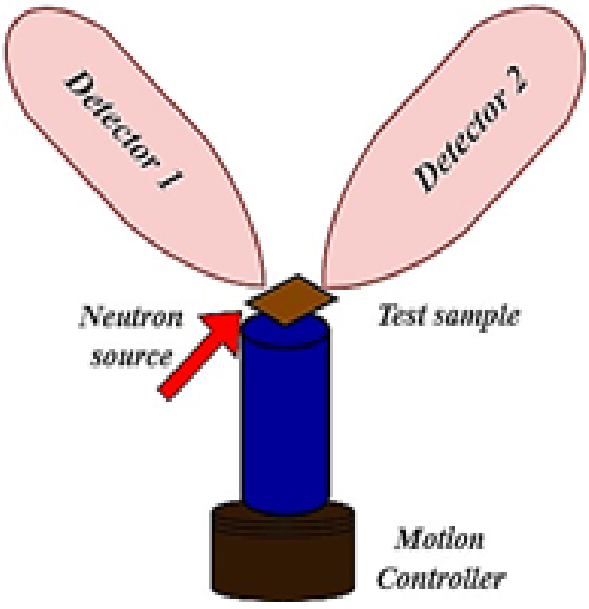



**Figure 5.** Setup for neutron diffraction: A schematic.

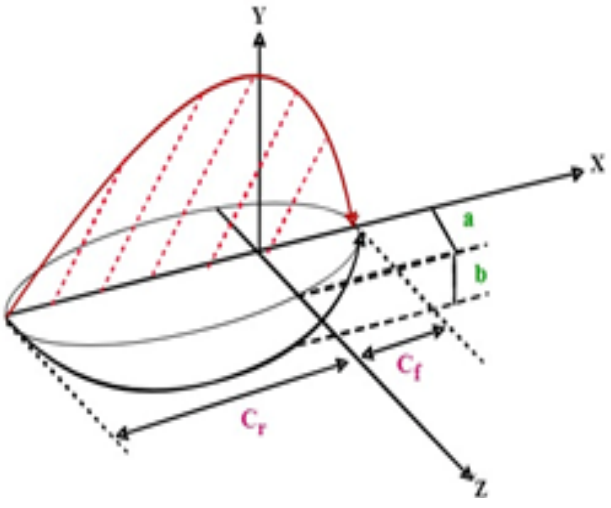



**Figure 6.** Schematic of Goldak twin semi-ellipsoidal heat source.

and stress evolution, therefore residual stresses as well as distortions.

Vacuum Assisted Resin Transfer Moulding (VARTM)[31] is used to make wind turbine blade root inserts. This work optimises the cure phase for several aims. Purely thermal performance analysis produces a Pareto front when thermal overshoot is necessary. Using a Finite Element (FE) simulator connected to a MO Genetic Algorithm, the Pareto sets of a coupled thermo-mechanical issue were addressed to provide optimum designs. The case study found that spring-in could have been decreased by 60% using the spring-in reduction technique instead of the overshoot temperature strategy. Transverse residual stress study includes a well-planned curing procedure.

A research proposed an unique linked thermal fluid mechanical approach[32] of stress development by merging CFD and FEM models. When compared to the thermal-mechanical model of the process, this one may provide a more accurate temperature field. Stress evolution in Wire-Fed Laser Additive Manufacturing (WFLAM) was analysed using a thermal fluid mechanical method. The novel thermal fluid mechanical model showed morphology's influence on stress. Simulations reveal that surface forming quality affects residual stress. The deposit's sidewall angle affects the residual Mises stress. This model properly predicts cracking by considering stress distribution during formation. Thermo-elastoplastic theory may be used to describe the temporal evolution of the temperature field in Equation (3) as follows:

$$C_p\rho\frac{dT}{dt}=\frac{\partial}{\partial x}\left(F\lambda_x\frac{dT}{dx}\right)+\frac{\partial}{\partial y}\left(F\lambda_y\frac{dT}{dy}\right)+\frac{\partial}{\partial z}\left(F\lambda_z\frac{dT}{dz}\right)+Q \quad (3)$$

A significant challenge for metal additive manufacturing is the need to adapt process-structure-property techniques now under development to practical, complex geometries. Microstructure and, consequently, mechanical characteristics and residual stresses, as required for precise evaluation and planning for structural stability, such as fatigue cracking, are of particular concern in the current work, and thus the need for objects based on such realistic configurations of thermal records is of particular importance. The new model[33] exhibits considerably better cooling rate agreement, a crucial factor in phase transition prediction, making modelling of complicated engineering components more practical. By incorporating the familiar Goodman formula for the impact of mean stress to Basquin's equation[33], we obtain the relationship between fatigue life $N_f$ and stress range, mean stress, and residual stress as given in Equation (4).

$$N_f=\left[\frac{\sigma_a}{\sigma_f'\left(1-\frac{\sigma_m+\sigma_r}{\sigma_{TS}}\right)}\right]^{\frac{1}{b}} \quad (4)$$

where $\sigma_f'$ and b are high-cycle fatigue material constants, known as fatigue strength coefficient (MPa) and exponent, respectively, $\sigma_a$ is alternating stress (MPa), is mean stress (MPa), $\sigma_r$ is residual stress (MPa) and $\sigma_{TS}$ is ultimate tensile strength (MPa). It should be emphasized that various AM process parameters can result in varying mechanical properties and fatigue behaviour.

The impacts of power input, penetration depth distance, raster hatch scan spacing, porosity of powder, and re-melt volume on temperature outline, stress development, and re-melt volume were analysed using a three-dimensional thermo-mechanical modelling[34] of the Electron Beam Additive Manufacturing (EBAM) process on AISI 316L stainless steel is shown in Table 1. To represent the heat flow between the electron beam and the powder, we use the Gaussian distribution function with an in-plane 'Qin,' as indicated in Equation (5). In this research, a three-dimensional Finite Element Model (FEM) of an EBAM process is developed for the purpose of examining the metal part's mechanical and thermal properties. The amount of re-melt is decreased by increasing the hatch spacing between raster patterns. Heat transmission, phase change, and thermal stress are all modelled in the system to characterise phase evolution. Uncertainty quantification and kinetic Monte Carlo simulations are two statistical methods that may be used to determine how much input process parameter variability affects the microstructure and mechanical/thermal performance of the 3D printed specimen.

$$Q_{in}=\left(\frac{2aP_{in}}{\pi w^2}\right)\left[e^{\frac{-2(x^2+y^2)}{w^2}}\right]\left(1-\frac{z}{d}\right) \quad (5)$$

Analytical model[35] proposed to account for thermo-viscoelastic effects on thin-walled curved composites during curing. Viscoelastic effects owing to radial and

**Table 1.** Input process parameters used to model the beam power distribution[34]

| Process parameters | Value/range |
|---|---|
| Beam spot size (ω) | 75 µm |
| Beam power (Pin) | 150 W |
| Coefficient of absorption (a) | 0.7 |
| Penetration depth (d) | 70-90 µm |

tangential thermal-chemical expansion on residual stresses and spring-in are separately studied. Curved composite materials cured on a wound carbon-epoxy tubular tool show excellent agreement between analytical findings and practical data and viscoelastic FEA predictions. An ANSYS User MAT subroutine for performing viscoelastic finite element analyses has been written. When comparing the difference in tangential thermo-chemical expansion between plies and radial thermo-chemical growth, the analytical CHILE constitutive law yields findings that are 38% and 10% bigger, respectively, than the viscoelastic model. Compared to CHILE[36] constitutive law., the residual stresses for cross-ply composite components are 38% lower when using the proposed analytical model to viscoelastic constitutive law. This is because of the tangential thermal-chemical strain mismatch between plies.

Temperature-dependent residual stresses in Fiber-Reinforced Polymers (FRP)[37] tubes are studied. FRP tube manufacturing considers "cooling temperature", "carbon -nanotubes CNT reinforcement", and "tube size". This study demonstrates that FRP laminate stresses in the depth and through-thickness directions may be predicted using slitting. Residual thermal stresses may be affected by several parameters. This research aims to characterise the thermo-mechanical influences on the residual stress of FRP composite tubes. Slitting[38] was used to assess composite tube's non-uniform residual stresses. Outer layers of all specimens investigated showed tensile thermal residual stresses, whereas interior layers showed compressive stresses. In accordance to bending behaviour, which includes tensile and compressive pressures on the outer and inner surfaces, we see this shows how bending affects stress in circular cylinders. Using the strains that were measured, the residual stresses from the slitting experiment could be calculated as in Equation (6).

$$\varepsilon_{yy}(a_i) = \int_0^{a_i} G(x, a_i)\, \sigma_{yy}(x)\, dx \qquad (6)$$

Where $\varepsilon_{yy}(a_i)$ and $\sigma_{yy}(x)$ are measured strains and unknown residual stresses, respectively.

A sequentially coupled thermo-mechanical model[39] reproduces the distribution of residual stresses in laser-welded DP600 dual-phase steel. Adding the proposed hardening term, strain rate sensitivity model, and temperature measurement methodology improves the outcomes. Investigate the effects of annealing on the pattern of residual stresses. The amount of residual stress after annealing tends to rise at higher temperatures. Laser welding efficacy is measured using a well calibrated simulation model. Distribution area is increased using laser welding, while residual stresses are unaffected. The findings of a simulation study of laser welding performed using martensitic elastic characteristics for the weld are quite similar to those obtained with a model employing the elasticity of dual phase steel DP600 as the foundation metal. The comparable plastic strains and von Mises residual stresses left behind after annealing rise as the temperature is raised. Weld residual stresses are modified by the annealing temperature. Variations in von Mises residual stresses all along welding transversal route may be seen at the fusion zone and 10mm from the weld line when using laser welding simulations using the Johnson-Cook thermal sensitive model[40] and the suggested model.

Several arithmetical simulation tools predict and reduce part distortion. SLM with several powder tracks is simulated using a thermo-mechanical model[41] provided by the aforementioned research. Finite-element modelling incorporates all three phases of solidification, melting, and cooling. A relocating, volumetric heat source has been included into the thermal analysis. To extrapolate residual stresses from temperature differences, the mechanical analysis employs an elasto-plastic constitutive law. Thermal and mechanical characteristics of materials are influenced by temperature. The purpose of this research is to ascertain whether or not there is a correlation between the scan approach and the residual stresses of the components. Temperature, thermal stress,

and residual stress may all be anticipated in printed parts using the suggested method. The differential equation for transient heat conduction inside a continuous medium of arbitrary dimension may be derived using the first law of thermodynamics. The following statement is developed from the solution of a heat Equation (7) that describes the Temperature T as a function of the time t:

$$k\left(\frac{\partial^2 T}{\partial x^2}+\frac{\partial^2 T}{\partial y^2}+\frac{\partial^2 T}{\partial z^2}\right)+\dot{q}=\rho c_p\frac{\partial T}{\partial t} \quad (7)$$

Where k represents thermal conductivity, is mass density, $c_p$ represents specific heat, and q represents power density in the work piece. The apparent specific heat is calculated by rearranging the specific heat between the solidus and liquidus temperatures to serve as the foundation for apparent specific heat[42] not all heat sources were accounted for in the simulation. The ability to estimate mechanical residual stresses properly requires a model that incorporates transient thermal behaviour. Two residual stress scan methodologies are compared numerically. There is a tight connection between the reality of temperature fluctuations and the mechanical reaction.

Through the use of process history in conjunction with inherent strain, the inherent strain technique may assess the distribution of ultimate stresses in a single mechanical step. By adjusting the Modified Inherent Strain[43] (MIS), technique for AM, a strategy for evaluating mechanical property variation during AM (MIS-AM) is proposed. For various process parameters and heat source pathways, the proposed MIS-AM approach is consistent to a published experiment and a full thermo-mechanical model. Predictions of stresses and deformations using the MIS technique rely on precise mechanical characteristics. Virtual machines with high MIS accuracy outperform MIS models with consistent attributes by a factor of 10%. High computational efficiency of the suggested model is encouraging for topology or processes parameter optimization. In this study, we present MIS-AM, a method for taking mechanical property variation in metal AM into account. As compared to a more in-depth thermomechanical model, MIS-AM performs better. An optimization process may benefit from the MIS-AM method's enhanced computing efficiency, since it only takes seconds to simulate a single layer with a length measured in meters.

Aerospace tolerances may be fulfilled in the production of thin-walled, axisymmetric elements by using a stringent LPBF process design in conjunction with pre- and post-process operations. Despite substantial residual stresses that induce distortion during LPBF manufacture and after cut-off. To do so, the LPBF method and pre- and post-processing must be carefully designed. Using stress relief annealing[44] spike in distortion shortly after cut-off is eliminated because to the high temperature fluctuation (1150°C/6 h) high-symmetry stator vanes are possible. For 90% of the part's surface, the cumulative dimensional deviation was reduced by over three times, and for 98%, it was reduced by almost twice. For pre-deformed products, stress relief annealing is recommended regardless of any differences in dimensions.

The study examines the residual stresses on High Pressure Nozzle Guide Vane (HPNGV)[45] component with and without the base plate in SLM. ANSYS software was used to construct a thermo-mechanical FEM for SLM-processed Inconel HPNGV. Experimental X-ray diffraction[46] determined residual stresses. Location 4's highest residual stress was 700 MPa. After base plate removal, SLM-processed HPNGV parts had greater residual stresses. After base plate removal, residual stress increases by 16% at site 4 and 27% at location 2. Sample experiments matched FEM simulation findings. The thermal stresses involved in an elasto-plastic process. An expression for thermal strain is shown in Equation (8):

$$\varepsilon^{th}=\alpha_e\Delta T=\alpha_e\left(T-T_{ref}\right) \quad (8)$$

where;

$T_{ref}$ - Reference temperature as a point of at t = 0.

$\alpha_e$ - thermal -Expansion Coefficient

$\varepsilon^{th}$ - Thermal strain

So, effective stress can be written as:

$$\sigma_{eff}=\sqrt{\sigma_1^2+\sigma_2^2+\sigma_3^2}+2\theta(\sigma_1\sigma_2+\sigma_1\sigma_3+\sigma_2\sigma_3) \quad (9)$$

$\sigma_1$, $\sigma_2$ and $\sigma_3$- Three principal stresses.

Looking into the differences between the residual stresses predicted by finite element analysis and those seen in experiments. The range and general pattern of the residual stresses found in the simulation are quite close to

those found in the experiments. The removal of the base plate increases the residual stresses in both simulations and experiments. HPNGV is a more substantial piece that doesn't change shape or size when separated from the base plate; this allows for the discharge of residual stresses.

We put the computational model[47] of multi-bead SS316L deposition to the test by using experimental clad bead sizes and process parameters. Zigzag techniques were used to build an experimental rectangular clad coating on a substrate 3 mm thick, proving the theoretical model correct. The numerical findings were consistent with the infrared & X-ray diffraction data. This model improves Laser Aided Additive Manufacturing (LAAM) knowledge by permitting industrial scanning algorithm selection. The model and insights may be used to manage residual stress, distortions, and microstructure for larger LAAM sections. A three-dimensional thermomechanical model for LAAM route planning was given. Continuous deposition was predicted via simulation approaches. With each simulation phase, a new domain was introduced, with its physical elements active alongside laser movement. LAAM scanning patterns are analysed using the thermo-mechanical model. Based on this result, researchers may investigate more complicated LAAM geometry in several layers to produce stronger scanning pattern selection criteria. This study emphasises the importance of bigger area LAAM deposition and 3D LAAM component manufacturing.

The research studied L-PBF residual stress using Simufact Additive FE thermo-mechanical[48] modelling. Actual powder and voxel modelling were used to save simulation time and imitate the genuine process. Gleeble 3800 testing at high temperatures calibrated FE simulation correctness. The calibrated model checked residual stress after removing supports. XRD confirmed simulations. 97% of simulations match experiments. Residual stress modelling using a thermomechanical approach. Complex gas/steam turbine designs may benefit from the foresight provided by the residual stress simulation thermo-mechanical model and material property calibration method. The effect of layer thickness change upon residual stress was measured using a calibrated model after a component was removed from the bottom plate. With reference to Equation (10), the intensity of a Gaussian volumetric heat source is denoted by Q. In this Equation, P represents laser power,  represents the laser spot radius and r represents the radial distance

$$Q(r) = \frac{2P}{\pi r_0^2} exp - \frac{2r^2}{r_0^2} \quad (10)$$

A thermo-mechanical model[49] was generated in this research to analyse the effects of thermal residual stresses on a one-layer AlSi10Mg part produced using direct metal laser sintering. The model is verified by thermal strain analysis. Both the intensity and velocity of the laser had an effect on the thermal residual stresses. The expansion and contraction brought on by changes in temperature also leads to discolouration and thermal residual tension. The goal of this study is to improve processing parameters to minimise thermal residual stress. In this study, a thermo-mechanical model for direct metal laser sintering of AlSi10Mg powder is proposed for the analysis of thermal residual stresses. Simulations ANSYS 17.0 The amount of residual heat is affected by the power and scan speed. The numerical model was verified using theory and analysis. The model analysed how the parameters of laser power and scan speed affected thermal residual stress and strain. The model is verified by thermal simulation. The model must have the capability to produce AM components and estimate thermal residual stress.

The influence of thermomechanically related effects on FG coating-substrate shakedown maps is unclear. The shakedown map's friction coefficient and yield stress might vary with temperature, hence a mathematical optimization technique[50] be provided for their development. Both the elastic completion of the development limit and the elastic limit are reduced by friction heat, and the declines are exacerbated by the sliding velocity. Surface tensile tension might increase and compressive stress could decrease as a result of friction heat. At high friction coefficients, the elastic limit and shakedown limit may benefit from a decrease in the distribution gradient index. In order to build the shakedown map of a two-dimensional FG coating-substrate system, this research creates a piecewise-constant strategy with temperature-dependent yield stress and friction coefficient. A mathematical model of the elastic shakedown limit and the elastic limit is built using Melan's static shakedown theorem; this model takes into account the temperature dependence of the friction coefficient and the yield stress.

In the research, we construct a Directed Energy Deposition (DED) Thermo-Mechanical-Metallurgical (TMM) FE models in ABAQUS/CAE. In addition to foreseeing temperature histories, residual stress, substrates deformation, and metallurgical phase fractions, this model also includes solid-state transformation stresses directly in the mechanical analysis. In this study, we explain the methodology used, the findings, and the experimental validation of a TMM Fe model[51] analysis of DED-processed 42CrMo4 steel. An infrared camera was also used to assess the melt pool region and the findings were compared to the FE findings. The mechanical analysis performed in the heat transfer study included the phase fractions determined in the metallurgical analysis. The lack of martensitic dwell time was shown to result in slower cooling rates. The cantilevered substrate eliminates heat outflow without requiring additional dwell time, which is a problem with bigger, permanently installed substrates. Changing this may affect how quickly the printed alloy cools and its overall qualities.

Feed-Water Valves[52] (FWVs) control the flow of water through steam turbines. Valve bodies may be weakened by overheating and pressure. Valve bodies are subjected to mechanical and thermal stress tests. The opening degree increases the high-velocity zone. Maximum valve stress satisfies design specifications. This study aids in the design of FWVs and related valves.

The welding heat cycle in Twinning Induced Plasticity (TWIP)-Ti Thermo-mechanical simulations of steel were performed using a finite element model[53]. XRD measurements in crucial welding areas validated residual stress estimates. A residual Stress Critical Zone (SCZ) was created based on fusion zone and Heat-impacted Zone residual stress and hardness (HAZ). TWIP-Ti yield strength SCZ residual stresses Weld joints were prepared and restrained to reduce residual stress and distortion. Micro hardness and residual stress were used to define SCZ. Weld structural integrity was measured by comparing SCZ stress to TWIP-Ti steel YS. A finite element model[54] laser metal depositing additive manufacturing's thermal domains, residual stresses, and distortions. Residual stresses and deformation are computed based on the results of a transient heat transfer study. To predict the evolution of temperature distributions, this work calibrates and uses a numerical thermal model. In order to lessen residual stresses and structural distortions, a numerical process optimization was used. With the analysis of heat transfer mechanically connected, residual stresses and deformation are reduced when model predictions are gradually extended to the new conditions.

Laser fusion of powder beds specimens are heat treated between 800°C and 950°C, and their fatigue strength is examined. Defects and residual strains may be studied by CT and X-ray diffraction. Certain batches showed less residual stress following stress reduction. Strength and fatigue resistance of notches are both increased by surface compressive residual stresses, which reduce the likelihood of fatigue cracking. Temperature has an effect on length, energy use, and resistance to exhaustion. The study's objective is to locate the minimum temperature conducive to full martensitic transformation[55] provides sufficient ductility to fulfil ASTM minimum possible elongation standards without sacrificing the material's maximum tensile or fatigue strength. The second aspect of the research is a look into the impact of spinning residual stresses on fatigue strength in both the plain and notch configurations. After machining, experimental batches were heat-treated to minimise stress. Both microstructures after heat treatment are equivalent. There are no flaws or residual strains in thermomechanically treated Ti-6Al-4V[56]. After heat treatment, the fatigue life of additively made samples is less than half that of thermomechanically treated samples. Microstructure influences Ti-6Al-4V ratcheting before and after heat treatment. Longer annealing reduces the low cycle fatigue life of Ti-6Al-4V compared to thermo-mechanically processed material with identical tensile characteristics. Multi-variant martensitic enhances the fracture propagation resistance and fatigue life of additively manufactured materials. WAAM stress was alleviated by induction heating. Heat treatment is a flexible intermediate step in WAAM or hybrid production. Based on stress changes, component shape, processing parameters and heat treatment, a finite element model anticipates the thermal and stress field during WAAM and induction heating[57]. Simulation results, component qualities, and application requirements all have an impact on stress distribution. The process benefits from thermal and stress testing of the C-beam WAAM component. Stress was distributed more evenly thanks to induction heating. There is an effect of induction heating on

**Table 2.** Summary of different modelling approaches according to different feedstocks and MAM processes

| Thermal Modelling Approaches | Feedstock | Metal Additive Processes | Observing Parameters | References |
|---|---|---|---|---|
| Thermo-mechanical material plasticity model | dual phase DP600 steel | laser welding process | Material anisotropy, Residual Stresses (RS) | 26 |
| Multi-material approach | Alumina ceramics, Alumina-zirconia | Lithography-based Ceramic Manufacturing technology (LCM) | Designing complex-shaped ceramic architecture | 27 |
| Computational modelling | Ni-based super alloys | Laser-beam and electron-beam AM processes | Crack initiation methods | 28 |
| Semi-analytical thermal approach | Mild steel, titanium, and aluminium | Laser Powder Bed Fusion (LPBF) | Temperature history, RS and distortion | 30 |
| Thermal fluid mechanical model | Ti-6Al-4 V | Wire feeding-based laser additive manufacturing | Stress evolution | 32 |
| Three-dimensional finite element modelling | Ti-6Al-4V | Powder Bed Fusion (PBF) | Scanning strategy upon temperature distribution history and residual stresses | 33 |
| Transient thermo-mechanical modeling | AISI 316L stainless steel | Electron beam additive manufacturing | Temperature distribution profile, stress development and re-melting volume | 34 |
| Thermo-viscoelastic analytical model | Fiber-reinforced polymer | ANSYS with a User MAT subroutine | RS and spring-in angles in components | 35 |
| Thermo-elasto-plastic constitutive model | Dual phase DP600 steel | Laser welding process | Strain rate and temperature influence on FEM residual stresses | 39 |
| Thermo-mechanical model | Ti-6Al-4V | Selective Laser Melting Process | Scan strategy on the residual stresses | 41 |
| Modified inherent strain model | Mild steel S355 | Powder Bed Fusion method, PBF | RS and deformations | 43 |
| Inherent strain method | Inconel 718 | Laser Powders Bed Fusion (LPBF) | Microstructure and properties using heat treatments | 44 |

| | | | | |
|---|---|---|---|---|
| Thermo-mechanical modelling approach | Inconel 718 | Selective Laser Melting Process | Residual stress prediction | 45 |
| Material Extrusion (MEX) | MEX fabricated thermoplastic | MEX | Residual strain measurement | 25 |
| Computationally efficient method | Multi-bead SS316L | Laser aided additive manufacturing | Influence of scanning patterns in LAAM process | 47 |
| Thermo-mechanical approach | Inconel 718 | Laser additive manufacturing | Residual stress evolution | 48 |
| Thermo-mechanical modeling | AlSi10Mg | Laser powder bed fusion | Validation of stress field | 49 |
| Thermo Mechanical-Metallurgical (TMM) Finite Element (FE) model | 42CrMo4 steel - a medium carbon alloy | Directed Energy Deposition (DED) | Temperature history, residual stress, substrate distortion and metallurgical phase fractions | 51 |
| Finite element simulation model | Twinning Induced Plasticity (TWIP) steel micro alloyed with titanium | Gas Tungsten Arc Welding (GTAW) | Numerical prediction of residual stress | 53 |
| Thermo-mechanical analysis | Al-Mg alloys | Wire-based laser metal deposition | RS and deformations | 54 |
| Finite element simulation | Ti–6Al–4V alloy | ABAQUS UHARD subroutine | Heat treatment microstructures of comparable mechanical properties | 56 |
| Elastic–plastic material model | Heat-treated AlSi10Mg | Laser Powder Bed Fusion (LPBF) | Lattice structures Material characterisation | 59 |
| Thermo-mechanical relaxation | Inconel 718 | Shot peening | Compressive residual stresses | 58 |

WAAM parts. Due to induction heating, WAAM stress is decreased. The analogous heat source model based on coils is used to mimic the induction heating thermal field. Both induction heating and WAAM are capable of predicting the stress levels before and after heating.

Shot peening's ability to generate residual stresses with a compressive character[58] Boost Energy Despite Fatigue. Residual stresses after initial compressive shot peening may be reduced via cyclic mechanical, thermal, or thermo-mechanical loading. When trying to anticipate weariness, it's crucial to unwind since doing so increases fatigue resistance. A numerical approach was developed to examine the High Cycle Fatigue (HCF) behaviour of shot-peened parts. Shot peening was used to modify surface

properties throughout the first mechanical, thermal, and thermo-mechanical cycles. By testing the current design with a shot-peened Inconel 718 part, we were able to verify its efficacy. The outcomes of the experiments were consistent. Engineers may use this technique to better foretell the HCF of shot-peened parts and hence optimize production. The overall different modelling approaches are summarised in the Table 2.

## 4.0 Conclusion

Additive manufacturing process numerical models are a low-cost, high-precision method for foreseeing product quality. These models are a cheap substitute for costly experiments that would have hampered quality control and component optimization. To show one's work and methods Analysis of commercial printer performance may make use of reduced-order or substitute models. This article describes the procedures, descriptions, and various factors that influence residual stresses. Several observations may be drawn from this:

- Because of its higher computer efficiency, the Modified Inherent Strain (MIS) technique may be used to optimise mechanical parameters in order to forecast stresses and deformations.
- Model predicts cracking based on an investigation of formation stress. Thermo-elastoplastic theory may be used to explain the development of the temperature field over time enabling easier modelling of sophisticated engineering elements. Using a variety of materials, 3D printing technology was used to create complicated ceramic structures.
- When hatches are placed farther apart, less re-melt is created. To account for phase development, heat transfer, phase change, and thermal stress are all modelled.
- Temperature has an effect on both thermal and mechanical characteristics. We look at how the scanning approach affects residual stresses. The method can forecast component temperatures, stresses, and residual stresses.
- The modelling findings forecast with each simulation iteration, a new domain with dynamic, physical and laser components was created. A thermomechanical model is used to analyse LAAM scanning patterns. Residual stress simulations anticipate and analyse residual stress in gas/steam turbine systems by combining a thermomechanical model with material property calibration.
- Mechanically analysing the percentages of metalworking steps. Cooling was delayed by time spent at marten sites. Heat cannot be dispersed by cantilevered substrates. The characteristics and cooling rates of the alloy may fluctuate.
- Optimisation resulted in fewer residual stresses in the structure. Using coupled heat transfer analysis reduces stress and deformation.
- The purpose of this research is to determine the minimal temperature necessary to achieve a complete martensitic transition and adequate ductility to meet ASTM minimum total elongation criteria without compromising maximum tensile and fatigue strength.
- The heat field of induction heating is displayed. Pressure is reduced through induction heating and WAAM.
- Shot-peened components with high-cycle fatigue were measured. Shot peening. Surfaces were mechanically, thermally, and thermomechanically shot-peened.

The outcomes of this study provide a thermal modelling of residual stresses and AM recommendations. This study's modelling of residual stresses is a step toward enhancing the practicality of AM printing and components.

## 5.0 References

1. Bartlett JL, Croom BP, Burdick J, Henkel D, Li X. Revealing mechanisms of residual stress development in additive manufacturing via digital image correlation. Addit Manuf. 2018; 22:1-12. https://doi.org/10.1016/j.addma.2018.04.025
2. Singh UP, Swaminathan S, Phanikumar G. Thermo-mechanical approach to study the residual stress evolution in part-scale component during laser additive manufacturing of alloy 718. Mater Des [Internet]. 2022; 222:111048. Available from: https://linkinghub.elsevier.com/retrieve/pii/S0264127522006700 https://doi.org/10.1016/j.matdes.2022.111048
3. Zhao L, Santos Macías JG, Dolimont A, Simar A, Rivière-Lorphèvre E. Comparison of residual stresses obtained

by the crack compliance method for parts produced by different metal additive manufacturing techniques and after friction stir processing. Addit Manuf. 2020; 36(July). https://doi.org/10.1016/j.addma.2020.101499

4. Ahmad B, van der Veen SO, Fitzpatrick ME, Guo H. Residual stress evaluation in selective-laser-melting additively manufactured titanium (Ti-6Al-4V) and inconel 718 using the contour method and numerical simulation. Addit Manuf. 2018; 22(March):571-82. https://doi.org/10.1016/j.addma.2018.06.002
5. Wang Q, Ji B, Fu Z, Xu Z. Experimental study on the determination of welding residual stress in rib-deck weld by sharp indentation testing. Thin-Walled Struct. 2021; 161(October 2020). https://doi.org/10.1016/j.tws.2021.107516
6. Ibrahim Mamane AS, Giljean S, Pac MJ, L'Hostis G. Optimization of the measurement of residual stresses by the incremental hole drilling method. Part I: Numerical correction of experimental errors by a configurable numerical-experimental coupling. Compos Struct. 2022; 294(May). https://doi.org/10.1016/j.compstruct.2022.115703
7. Beghini M, Bertini L, Mori LF. Evaluating non-uniform residual stress by the hole-drilling method with concentric and eccentric holes. Part II: Application of the influence functions to the inverse problem. Strain. 2010; 46(4):337-46. https://doi.org/10.1111/j.1475-1305.2009.00684.x
8. Mahmoodi M, Sedighi M, Tanner DA. Investigation of through thickness residual stress distribution in equal channel angular rolled Al 5083 alloy by layer removal technique and X-ray diffraction. Mater Des. 2012; 40:516-20. https://doi.org/10.1016/j.matdes.2012.03.029
9. Marola S, Bosia S, Veltro A, Fiore G, Manfredi D, Lombardi M, *et al*. Residual stresses in additively manufactured AlSi10Mg: Raman spectroscopy and X-ray diffraction analysis. Mater Des. 2021; 202. https://doi.org/10.1016/j.matdes.2021.109550
10. Yang F, Jiang JQ, Fang F, Wang Y, Ma C. Rapid determination of residual stress profiles in ferrite phase of cold-drawn wire by XRD and layer removal technique. Mater Sci Eng A. 2008; 486(1-2):455-60. https://doi.org/10.1016/j.msea.2007.09.025
11. Prevéy PS. Current applications of XRD diffraction residual stress measurement. Dev Mater Charact Technol ASM Int. 1996; (513):103-10.
12. Liang L, Hu R, Wang J, Huang A, Pang S. A thermal fluid mechanical model of stress evolution for wire feeding-based laser additive manufacturing. J Manuf Process. 2021; 69(May):602-12. https://doi.org/10.1016/j.jmapro.2021.08.008
13. Yuan Z, Wang Y, Yang G, Tang A, Yang Z, Li S, et al. Evolution of curing residual stresses in composite using multi-scale method. Compos Part B Eng. 2018; 155(July):49-61. https://doi.org/10.1016/j.compositesb.2018.08.012
14. Ferreri NC, Feng Z, Savage DJ, Brown DW, Clausen B, Sisneros TA, *et al*. In-situ high-energy X-ray diffraction and crystal plasticity modeling to predict the evolution of texture, twinning, lattice strains and strength during loading and reloading of beryllium. Int J Plast. 2022;150(September 2021). https://doi.org/10.1016/j.ijplas.2022.103217
15. Doumenc G, Couturier L, Courant B, Paillard P, Benoit A, Gautron E, *et al*. Investigation of microstructure, hardness and residual stresses of wire and arc additive manufactured 6061 aluminium alloy. Materialia [Internet]. 2022; 25:101520. Available from: https://linkinghub.elsevier.com/retrieve/pii/S2589152922002022 https://doi.org/10.1016/j.mtla.2022.101520
16. Li R, Xiong J, Lei Y. Investigation on thermal stress evolution induced by wire and arc additive manufacturing for circular thin-walled parts. J Manuf Process. 2019; 40(March):59-67. https://doi.org/10.1016/j.jmapro.2019.03.006
17. Tanaka H, Tanaka M. Main factors governing residual effective stress for cohesive soils sampled by tube sampling. Soils Found. 2006; 46(2):209-19. https://doi.org/10.3208/sandf.46.209
18. Manai A, Franz von Bock und Polach RU, Al-Emrani M. A probabilistic study of welding residual stresses distribution and their contribution to the fatigue life. Eng Fail Anal. 2020; 118(July). https://doi.org/10.1016/j.engfailanal.2020.104787
19. Han X, Li C, Liu Z, Chen X, Deng S. Analysis of residual stress distribution characteristics of laser surface hardening based on Voronoi model. Opt Laser Technol. 2022; 156(July):108613. https://doi.org/10.1016/j.optlastec.2022.108613
20. Wang F, Yang J, Azim I, Bai L, Ma Y. Experimental and numerical evaluations of the distribution and effect of roll-forming residual stress on CFS sigma beams. J Constr Steel Res. 2020;167. https://doi.org/10.1016/j.jcsr.2020.105978
21. Nishimura R, Kishimoto S, Sasaki T, Mitsui S, Shinya M, Arai Y, *et al*. Fine residual stress distribution mea-

surement of steel materials by SOI pixel detector with synchrotron X-rays. Nucl Instruments Methods Phys Res Sect A Accel Spectrometers, Detect Assoc Equip. 2020; 978(July). https://doi.org/10.1016/j.nima.2020.164380

22. Zhang H, Wang Y, Han T, Bao L, Wu Q, Gu S. Numerical and experimental investigation of the formation mechanism and the distribution of the welding residual stress induced by the hybrid laser arc welding of AH36 steel in a butt joint configuration. J Manuf Process. 2020; 51(January):95-108. https://doi.org/10.1016/j.jmapro.2020.01.008
23. Taraphdar PK, Kumar R, Giri A, Pandey C, Mahapatra MM, Sridhar K. Residual stress distribution in thick double-V butt welds with varying groove configuration, restraints and mechanical tensioning. J Manuf Process. 2021; 68(July):1405-17. https://doi.org/10.1016/j.jmapro.2021.06.046
24. Wu H, He D, Guo X, Gao M, Tan Z, Wang G. A segmented heat source for efficiently calculating the residual stresses in laser powder bed fusion process. J Manuf Process. 2022; 79(May):206-18. https://doi.org/10.1016/j.jmapro.2022.04.051
25. Wang S, Lasn K, Elverum CW, Wan D, Echtermeyer A. Novel in-situ residual strain measurements in additive manufacturing specimens by using the Optical Backscatter Reflectometry. Addit Manuf. 2020; 32(September 2019). https://doi.org/10.1016/j.addma.2020.101040
26. Liu S, Kouadri-Henni A, Gavrus A. Numerical simulation and experimental investigation on the residual stresses in a laser beam welded dual phase DP600 steel plate: Thermo-mechanical material plasticity model. Int J Mech Sci [Internet]. 2017; 122(July 2016):235-43. https://doi.org/10.1016/j.ijmecsci.2017.01.006
27. Schlacher J, Hofer AK, Geier S, Kraleva I, Papšík R, Schwentenwein M, *et al.* Additive manufacturing of high-strength alumina through a multi-material approach. Open Ceram. 2021; 5(February). https://doi.org/10.1016/j.oceram.2021.100082
28. Guo C, Li G, Li S, Hu X, Lu H, Li X, *et al.* Nano materials science additive manufacturing of Ni-based superalloys: Residual stress, mechanisms of crack formation and strategies for crack inhibition. 2022; (June). https://doi.org/10.1016/j.nanoms.2022.08.001
29. Dumas M, Fabre D, Valiorgue F, Kermouche G, Van Robaeys A, Girinon M, *et al.* 3D numerical modelling of turning-induced residual stresses- A two-scale approach based on equivalent thermo-mechanical loadings. Journal of Materials Processing Technology. 2021; 297. https://doi.org/10.1016/j.jmatprotec.2021.117274
30. Yang Y, Zhou X, Li Q, Ayas C. A computationally efficient thermo-mechanical model for wire arc additive manufacturing. Addit Manuf. 2021; 46(October 2020). https://doi.org/10.1016/j.addma.2021.102090
31. Pelegri AA, Kedlaya DN. Composites: Part A. Construction. 2008; 39(September):1433-43. https://doi.org/10.1016/j.compositesa.2008.05.006
32. Liang L, Hu R, Wang J, Huang A, Pang S. A thermal fluid mechanical model of stress evolution for wire feeding-based laser additive manufacturing. J Manuf Process. 2021; 69(August):602-12. https://doi.org/10.1016/j.jmapro.2021.08.008
33. Zhou J, Barrett RA, Leen SB. Three-dimensional finite element modelling for additive manufacturing of Ti-6Al-4V components: Effect of scanning strategies on temperature history and residual stress. J Adv Join Process. 2022; 5(March). https://doi.org/10.1016/j.jajp.2022.100106
34. Adhitan RK, Raghavan N. Transient thermo-mechanical modeling of stress evolution and re-melt volume fraction in electron beam additive manufacturing process. Procedia Manuf. 2017; 11(June):571-83. https://doi.org/10.1016/j.promfg.2017.07.151
35. Liu C, Shi Y. A thermo-viscoelastic analytical model for residual stresses and spring-in angles of multilayered thin-walled curved composite parts. Thin-Walled Struct. 2020; 152(February). https://doi.org/10.1016/j.tws.2020.106758
36. Arafath ARA, Vaziri R, Poursartip A. Closed-form solution for process-induced stresses and deformation of a composite part cured on a solid tool: Part II- Curved geometries. Compos Part A Appl Sci Manuf. 2009; 40(10):1545-57. https://doi.org/10.1016/j.compositesa.2009.01.009
37. Ghasemi AR, Asghari B, Tabatabaeian A. Determination of the influence of thermo-mechanical factors on the residual stresses of cylindrical composite tubes: Experimental and computational analyses. Int J Press Vessel Pip. 2020; 183(June 2019). https://doi.org/10.1016/j.ijpvp.2020.104098
38. Akbari S, Taheri-Behrooz F, Shokrieh MM. Characterization of residual stresses in a thin-walled filament wound carbon/epoxy ring using incremental hole drilling method. Compos Sci Technol [Internet]. 2014; 94(April):8-15. https://doi.org/10.1016/j.compscitech.2014.01.008

39. Liu S, Kouadri-Henni A, Gavrus A. DP600 dual phase steel thermo-elasto-plastic constitutive model considering strain rate and temperature influence on FEM residual stress analysis of laser welding. J Manuf Process. 2018; 35(May 2017):407-19. https://doi.org/10.1016/j.jmapro.2018.07.006
40. Huang Z, Gao L, Wang Y, Wang F. Determination of the Johnson-Cook constitutive model parameters of materials by cluster global optimization algorithm. J Mater Eng Perform. 2016; 25(9):4099-107. https://doi.org/10.1007/s11665-016-2178-1
41. Marques BM, Andrade CM, Neto DM, Oliveira MC, Alves JL, Menezes LF. Numerical analysis of residual stresses in parts produced by selective laser melting process. Procedia Manuf. 2020; 47(2019):1170-7. https://doi.org/10.1016/j.promfg.2020.04.167
42. Tchuindjang JT, Paydas H, Tran HS, Carrus R, Duchêne L, Mertens A, *et al*. A new concept for modeling phase transformations in ti6al4v alloy manufactured by directed energy deposition. Materials. 202; 14. https://doi.org/10.3390/ma14112985 PMid:34072987 PMCid:PMC8198765
43. Wang Y, Li Q, Qian L, Yang Y. A modified inherent strain model with consideration of the variance of mechanical properties in metal additive manufacturing. J Manuf Process. 2021; 72(August):115-25. https://doi.org/10.1016/j.jmapro.2021.09.059
44. Gruber K, Ziółkowski G, Pawlak A, Kurzynowski T. Effect of stress relief and inherent strain-based pre-deformation on the geometric accuracy of stator vanes additively manufactured from inconel 718 using laser powder bed fusion. Precis Eng. 2022; 76(November 2021):360-76. https://doi.org/10.1016/j.precisioneng.2022.04.007
45. Nagesha BK, Anand Kumar S, Vinodh K, Pathania A, Barad S. A thermo-mechanical modelling approach on the residual stress prediction of SLM processed HPNGV aeroengine part. Mater Today Proc. 2020; 44:4990-6. https://doi.org/10.1016/j.matpr.2020.12.940
46. van Zyl I, Yadroitsava I, Yadroitsev I. Residual stress in TI6AL4V objects produced by direct metal laser sintering. South African J Ind Eng. 2016; 27(4):134-41. https://doi.org/10.7166/27-4-1468
47. Ren K, Chew Y, Fuh JYH, Zhang YF, Bi GJ. Thermo-mechanical analyses for optimized path planning in laser aided additive manufacturing processes. Mater Des. 2019; 162:80-93. https://doi.org/10.1016/j.matdes.2018.11.014
48. Singh UP, Swaminathan S, Phanikumar G. Thermo-mechanical approach to study the residual stress evolution in part-scale component during laser additive manufacturing of alloy 718. Mater Des. 2022;222. https://doi.org/10.1016/j.matdes.2022.111048
49. Panda BK, Sahoo S. Thermo-mechanical modeling and validation of stress field during laser powder bed fusion of AlSi10Mg built part. Results Phys. 2019; 12(November 2018):1372-81. https://doi.org/10.1016/j.rinp.2019.01.002
50. Fu P, Zhao J, Zhang X, Kang G, Wang P, Kan Q. Thermo-mechanically coupled sliding contact shakedown analysis of functionally graded coating-substrate structures. Int J Mech Sci. 2022. https://doi.org/10.1016/j.ijmecsci.2022.107241
51. Cooke S, Sweet G, Ahmadi K, Bishop P, Herring R. Thermo-mechanical-metallurgical modelling, validation and characterization of 42CrMo4 steel processed by directed energy deposition. J Manuf Process. 2022; 81(May):537-61. https://doi.org/10.1016/j.jmapro.2022.07.007
52. Wen-Qing L, Zhao L, Yue Y, Jia-yi W, Zhi- Jiang J, Jin-Yuan Q. Thermo-mechanical stress analysis of feed-water valves in nuclear power plants. Nucl Eng Technol. 2022; 54(3):849-59. https://doi.org/10.1016/j.net.2021.09.018
53. García-García V, Mejía I, Reyes-Calderón F, Benito JA, Cabrera JM. FE thermo-mechanical simulation of welding residual stresses and distortion in Ti-containing TWIP steel through GTAW process. J Manuf Process. 2020; 59(September):801-15. https://doi.org/10.1016/j.jmapro.2020.09.042
54. Bock FE, Herrnring J, Froend M, Enz J, Kashaev N, Klusemann B. Experimental and numerical thermo-mechanical analysis of wire-based laser metal deposition of Al-Mg alloys. J Manuf Process. 2021; 64(February):982-95. https://doi.org/10.1016/j.jmapro.2021.02.016
55. Emanuelli L, Molinari A, Facchini L, Sbettega E, Carmignato S, Bandini M, *et al*. Effect of heat treatment temperature and turning residual stresses on the plain and notch fatigue strength of Ti-6Al-4V additively manufactured via laser powder bed fusion. Int J Fatigue. 2022; 162(January). https://doi.org/10.1016/j.ijfatigue.2022.107009
56. Ghosh A, Sahu VK, Gurao NP. Effect of heat treatment on the ratcheting behaviour of additively manufactured and thermo-mechanically treated Ti-6Al-4V alloy.

Mater Sci Eng A. 2022; 833(September 2021). https://doi.org/10.1016/j.msea.2021.142345

57. Shen H, Lin J, Zhou Z, Liu B. Effect of induction heat treatment on residual stress distribution of components fabricated by wire arc additive manufacturing. J Manuf Process. 2022; 75(December 2021):331-45. https://doi.org/10.1016/j.jmapro.2022.01.018
58. Seddik R, Seddik M, Atig A, Fathallah R, Infante V, Seddik M. Thermo-mechanical relaxation of compressive residual stresses induced by shot peening relaxation of compressive residual stresses Thermo-mechanical modeling of high turbine blade of an induced by shot peening airp. Procedia Struct Integr [Internet]. 2016; 2:2182-9. Available from: https://doi.org/10.1016/j.prostr.2016.06.273
59. Gebhardt U, Gustmann T, Giebeler L, Hirsch F, Hufenbach JK, Kästner M. Additively manufactured AlSi10Mg lattices - Potential and limits of modelling as-designed structures. Mater Des. 2022; 220. https://doi.org/10.1016/j.matdes.2022.110796